

Reverse Monte Carlo modeling of ion conducting network glasses: An evaluation based on molecular dynamics simulations

Christian R. Müller,^a Vindu Kathriarachchi,^b Michael Schuch,^c
Philipp Maass^{*c} and Valeri G. Petkov^b

Received 23rd February 2010, Accepted 26th April 2010

DOI: 10.1039/c003472j

We investigate the quality of structural models generated by the Reverse Monte Carlo (RMC) method in a typical application to glass systems. To this end we calculate diffraction data from a Li₂O–SiO₂ molecular dynamics (MD) simulation and use it, in addition to minimal pair distances and coordination numbers of silicon (oxygen) to oxygen (silicon) ions, as input for RMC modeling. Then we compare partial radial distribution functions, coordination numbers, bond angles, and ring sizes predicted by the RMC models with those of the MD system. It is found that partial distribution functions and properties on small lengths scales, as distributions of coordination numbers and bond angles, are well reproduced by the RMC modeling. Properties in the medium-range order regime are, however, not well captured, as is demonstrated by comparison of ring size distributions. Due care therefore has to be exercised when extracting structural features from RMC models in this medium-range order regime. In particular we show that the occurrence of such features can be a mere consequence of the chosen starting configuration.

1. Introduction

The Reverse Monte Carlo (RMC) method is commonly used to build structure models based on experimental data. Introduced by McGreevy and Pusztai in 1988,¹ it has been widely used and is now considered a standard method in analyzing structural data. Advantages of this method are its easy implementation and its wide applicability. It has been used to model various material systems such as crystals, polymers and glasses. In principle any structural data can be used as input for the RMC method, but most modelings focus on using diffraction data obtained from X-ray and/or neutron scattering. In ion conducting glass systems RMC models of the structure have been created for x Li₂S + (1 – x) SiO₂ glasses,² 0.7SiO₂ + 0.3Na₂O glass,³ x Na₂S + (1 – x)B₂S₃ glasses⁴ and 0.5Li₂S + 0.5[(1 – x) GeSe₂ + x GeO₂] glasses⁵ among others.

As pointed out by McGreevy, RMC models are “neither unique nor ‘correct’”, but can aid our understanding of local structure properties and their relation to other physical properties.⁶ It is important to study RMC models in different material classes and to get insight into the limits of the applicability of this method. One approach of testing the RMC method is to use structural data derived from computer simulations as input for the modeling and compare the resulting RMC structures with the original one. In the past, such

investigations have been undertaken for liquid argon and some molten salts,⁷ for colloidal aerogels⁸ and liquid chlorine.⁹

Similar tests become a more urgent question now in the case of more complex systems such as the ion conducting network glasses, where different types of atoms form a disordered glassy host matrix for mobile cations. In the RMC studies of these systems not only their short range order has been investigated, but also the medium range order. Among those studies are discussions of the rings sizes in vitreous SiO₂ and GeO₂,¹⁰ a detailed investigations of amorphous GeSe₂,^{11,12} and a proposal of a structural model for multi-component borosilicate glasses, where partial segregation of silicon and boron rich regions is predicted.¹³ It was also suggested to use such models as basis for further investigation of possible conduction pathways of the mobile ions. In this respect the RMC models have been employed in connection with geometric constraints and the bond valence (BV) analysis^{14,15} (see ref. 16 for a critical discussion of this procedure).

In this paper we test the RMC method against structural data generated from a molecular dynamics (MD) simulation of a Li₂O–SiO₂ glass. For this purpose we calculate diffraction data from the simulated MD structures and use it as input for the RMC modeling.¹⁷ For the evaluation of the resulting RMC models we determine how well various properties of the original MD structure are reproduced. Particularly we compare properties such as partial radial distribution functions and ring-size distributions, which are not easily accessible by experiment. Through our evaluation it can be clarified how far one can use the RMC method to gain insight into these properties, and where one need to be cautious before taking the features of the RMC model as real.

We want to stress that a testing based on the MD simulation is valid irrespective of whether it is a good representation of

^a Institut für Physik, Technische Universität Ilmenau, 98684 Ilmenau, Germany

^b Department of Physics, Central Michigan University, Mount Pleasant, Michigan 48859, USA

^c Fachbereich Physik, Universität Osnabrück, Barbarastraße 7, 49069 Osnabrück, Germany.

E-mail: philipp.maass@uni-osnabrueck.de;

Web: <http://www.statphys.uni-osnabrueck.de>

the real lithium silicate glass. Over the last few decades it has been established that simulated structures of such modified network glasses show no peculiarities, which make them basically different from the structures of real systems studied in experiments. It can, however, be difficult to generate all details of a structure in a simulation for a specific system. We will show that the RMC models generally compare well with the MD structure, but that one has to be careful when analyzing features of the medium-range order regime.

2. Molecular dynamics simulations

We perform MD simulations of a lithium silicate glass with the chemical formula $\text{Li}_2\text{O-SiO}_2$ using the potential model of Habasaki and Okada.¹⁸ The cubic simulation box has a length $L = 50.04 \text{ \AA}$ and contains 11664 atoms (3888 Li, 1944 Si, 5832 O) corresponding to a density of 2.27 g cm^{-3} and a number density of $\rho_0 = 0.093 \text{ \AA}^{-3}$. Periodic boundary conditions are used. The simulations are performed in the NVE ensemble (micro canonical ensemble where the number N of particles, the volume V of the simulation box, and the total energy E are kept constant). The energy E was adjusted so that the temperature of the system fluctuates around a mean value of 301 K with deviations of 2 K. The systems are equilibrated for about 1 ns and the runs for obtaining data have a duration of 2 ns, using a time step interval of $\Delta t = 1 \text{ fs}$.

The effective interatomic interactions between two atoms of type i and j at distance r are:

$$U_{ij}(r) = \frac{e^2}{4\pi\epsilon_0} \frac{z_i z_j}{r} + F_0(B_i + B_j) \exp\left(\frac{A_i + A_j - r}{B_i + B_j}\right) - \frac{C_i C_j}{r^6} \quad (1)$$

where the parameters listed in Table 1 have been optimized¹⁸ and shown to have good agreement with experimental data.¹⁸⁻²¹ The interaction potential in eqn (1) is composed of three terms. The first one in (1) is the Coulomb interaction with effective charge numbers for the species. The second term is a Born-Meyer type potential, which takes the short-range repulsive interactions into account, and the third is a dispersive van-der-Waals interaction. It is only used for interactions involving oxygen.

The system was initially thermalized at a high temperature 2500 K, which is well above the (computer) glass transition temperature of this system. From this liquid state the system is cooled down in several steps with intermediate periods of equilibration. First an NVT run (canonical ensemble, where the number N of particles, the volume V and the temperature T are fixed) of 10 ps at 2500 K is performed, followed by an NVE run of the same duration. After simulating another 20 ps in the NVT ensemble and 10 ps under NVE conditions the

Table 1 Potential parameters for the MD simulations (*cf.* eqn (1))

Ion	z	$A/\text{\AA}$	$B/\text{\AA}$	$C [\text{\AA}^3 \sqrt{\text{kJ/mol}}]$
Li^+	0.87	1.0155	0.07321	22.24
Si^{4+}	2.40	0.8688	0.03285	47.43
O^{2-}	-1.38	2.0474	0.17566	143.98
$F_0 = 4.186 \text{ kJ}\text{\AA}^{-1} \text{ mol}^{-1}$ $r_c = 1.3 \text{ \AA}$				

temperature is decreased in four subsequent sequences down to 300 K. Each cooling cycle consists of a 10 ps run using a thermostat to decrease the temperature linearly, a 10 ps NVT run at the target temperature, and a 10 ps NVE run to verify that there are no temperature drifts. The configurations at the end of the 300 K cooling cycle are used as starting points for a 800 ps long equilibration run using the NVE ensemble. The measuring runs are 2 ns long. All MD simulations were carried out with the LAMMPS software package.²²

The partial and total radial distribution functions $g_{ij}(r)$ and $G(r)$ as well as the total scattering structure factor $S(Q)$ were calculated according to the partial distribution function formalism (see ref. 23 for a discussion of different possible definitions of scattering functions). The partial radial distribution functions are given as

$$g_{ij}(r) = \frac{n_{ij}(r)}{4\rho_i\rho_j\pi r^2 dr}, \quad (2)$$

where $n_{ij}(r)$ is the average number of particles of type j between distances $r - dr/2$ and $r + dr/2$ from a particle of type i , and ρ_j is the mean number density of particles of type j .

The total radial distribution function $G(r)$ is calculated by

$$G(r) = 4\pi r \rho_0 \left[\sum_{i,j=1}^m [w_{ij} g_{ij}(r)] - 1 \right], \quad (3)$$

where ρ_0 is the total number density of all atoms in the system, m is the number of particle types, and w_{ij} are weighting factors:

$$w_{ij} = \left(\sum_{k=1}^m c_k \bar{b}_k \right)^{-2} c_i c_j \bar{b}_i \bar{b}_j. \quad (4)$$

Here $c_i = \rho_i/\rho_0$ are the molar fractions of particles of type i , and \bar{b}_i is their average bound coherent scattering length. In order to calculate X-ray diffraction functions one has to replace the \bar{b}_i with the atomic form factors f_i .

Finally, the total structure factor $S(Q)$ is calculated from $G(r)$ by

$$Q[S(Q) - 1] = \int_0^\infty G(r) \sin(Qr) dr. \quad (5)$$

All data from the MD system were averaged over 11 configurations from the 2 ns measurement run, which are 200 ps apart each. The scattering lengths and atomic form factors used in eqn (4) were taken from ref. 24 and 25, respectively, and are listed in Table 2. In the following we take the freedom to speak about these generated diffraction data simply as ‘‘diffraction data’’ and ask the reader to keep in mind that the data were not measured but calculated from eqn (2)–(5).

Table 2 Average bound coherent scattering lengths and atomic form factor for Li, Si, and O

	Li	Si	O
\bar{b}	-1.9	4.1491	5.803
f	3.005	14.41	8.144

3. Reverse Monte Carlo modeling

RMC simulations were carried out using the RMC++ package.²⁸ The simulations started with building an initial atomic configuration which was then refined against the $S(Q)$ and $G(r)$ data computed from the MD structure.

Two starting configurations were considered: a “random distribution” of atoms²⁹ (subsequently referenced by “R”) and another from the $\text{Li}_2\text{O-SiO}_2$ orthorhombic crystal structure (space group $Cmc21$, subsequently referenced by “C”). Both configurations consist of 3000 atoms (1000 Li, 500 Si, 1500 O) positioned inside a cubic box with a side length of 31.82 Å so that the atomic number density is the same as in the MD structure. From the random and crystalline-type starting configurations, two initial models “IR” and “IC” were prepared, respectively, by applying the following constraints:

(i) Si is coordinated fourfold with O using a minimal neighbor distance of 1.4 Å and a maximum neighbor distance of 1.8 Å. This corresponds to a 100% fraction $f_{\text{Si},\text{O}}(4) = 1$ of fourfold coordinated Si.

(ii) The relative numbers of bridging (two Si neighbors) and non-bridging oxygens (one Si neighbor) is 37 and 60%, respectively. This corresponds to $f_{\text{O},\text{Si}}(2) = 0.37$ and $f_{\text{O},\text{Si}}(1) = 0.60$.

(iii) Minimal atomic distances r_{min} given in Table 3 are required.

Intra-tetrahedral O-Si-O angles and inter-tetrahedral Si-O-Si angles were allowed to evolve freely. The preparation was run until the constraints (i)–(iii) were satisfied for at least 95% of the atoms (for given uncertainty parameters, see below).

After creating the initial models, the final refinement is done in order to obtain the best possible agreement between the computed $S(Q)$ and $G(r)$ from the RMC model and the calculated data from the MD-simulation. Both the real space as well as the reciprocal space data were used, since strong low- Q features in $S(Q)$ emphasize the medium range order, while $G(r)$ shows well defined low- r features which emphasize the short range atomic order. The same constraints as in the preparation of the initial models were applied also during the final RMC modeling.

In the modeling, the input quantities, *i.e.* the total radial distribution function $G(r)$, the total structure factor $S(Q)$, and the fractions $f_{\text{Si},\text{O}}(4)$, $f_{\text{O},\text{Si}}(2)$, and $f_{\text{O},\text{Si}}(1)$ of differently coordinated silicon and oxygen ions are taken into account by an effective Hamiltonian of type

$$H_{\text{eff}} = \sum_{\alpha} \chi_{\alpha}^2 = \sum_{\alpha} \frac{\tilde{\chi}_{\alpha}^2}{\sigma_{\alpha}^2}, \quad (6)$$

where $\tilde{\chi}_{\alpha}^2$ is the square deviation between the computed and the measured (in the case of constraints required) value of the input quantity α . The weighting (or tolerance) factors σ_{α} are summarized in Table 4. As in ordinary Monte-Carlo simulations, stochastic moves of the particles are performed

Table 3 Minimal atomic approach distances as used in the RMC modeling

Pair	Si-Si	Si-O	Si-Li	O-O	O-Li	Li-Li
$r_{\text{min}}/\text{Å}$	2.8	1.4	2.5	2.3	1.7	2.2

Table 4 Weighting factors σ_{α} used for the input quantities in the RMC modeling

Quantity	$S(Q)$	$G(r)$	$f_{\text{Si},\text{O}}(4)$	$f_{\text{O},\text{Si}}(2)$	$f_{\text{O},\text{Si}}(1)$
σ	10^{-6}	10^{-6}	10^{-4}	$10^{-3.5}$	$10^{-3.5}$

(while taking into account the minimum distance restrictions), which drive the ensemble of possible atomic configurations to a stationary state with probabilities $\propto \exp(-H_{\text{eff}})$. For details of the specific algorithm used in these simulations, we refer to the manual of the RMCA and RMC++ package, see ref. 30.

In total five RMC models were made. Models “XR” and “XC” were based on the random and crystalline-type starting configurations and refined against the X-ray data alone. Models “NR” and “NC” were based on the random and crystalline-type starting configurations and refined against the neutron data alone. A fifth model was made using both the X-ray and the neutron diffraction data and starting from the random configuration (“NXR”).

In Fig. 1 and 2 the corresponding total structure factors and total distribution functions are compared to the ones calculated from the MD structure. As expected, a good agreement is achieved through the RMC modeling.

4. Comparison of structural properties

4.1 Partial radial distribution functions

In Fig. 3 partial radial distribution functions $g_{ij}(r)$ (see eqn (2)) are shown. Generally the partial $g_{ij}(r)$ for S-Si, Si-O and Li-O generated by RMC and MD simulations agree well. However, in g_{OO} the second peak is lacking or too weakly pronounced in the RMC models. This difference can lead to significant

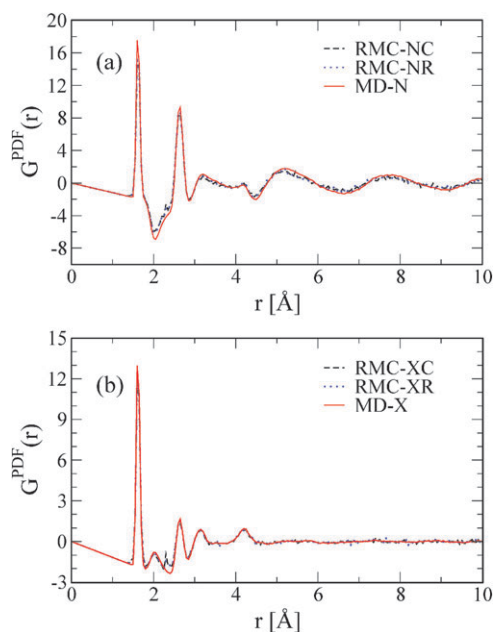


Fig. 1 Comparison of $G(r)$ of $\text{Li}_2\text{O-SiO}_2$ RMC models based on crystalline-type (dashed line) and random (dotted line) starting configurations with that of a $\text{Li}_2\text{O-SiO}_2$ MD system (solid line). Neutron diffraction data are shown in panel (a) and X-ray diffraction data in panel (b).

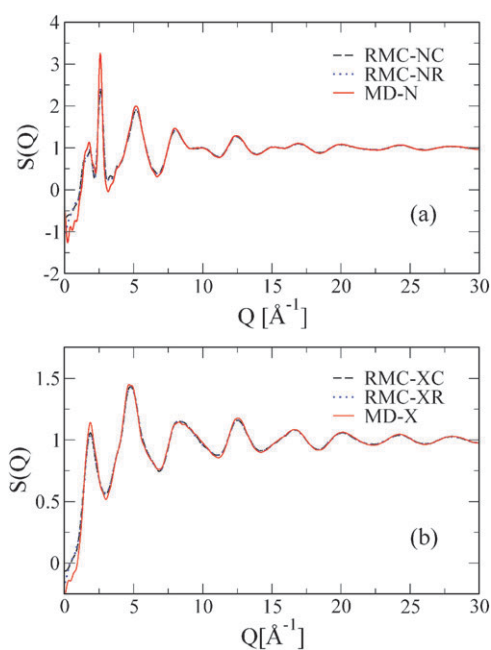


Fig. 2 Comparison of $S(Q)$ of $\text{Li}_2\text{O-SiO}_2$ RMC models based on crystalline-type (dashed line) and random (dotted line) starting configurations with that of a $\text{Li}_2\text{O-SiO}_2$ MD system (solid line). Neutron diffraction data are shown in panel (a) and X-ray diffraction data in panel (b).

deviations of the RMC generated models and the MD structure in the medium-range order regime (see also the discussion in section 4.4). While there is no dependence upon the starting configuration (crystalline or random), some differences can be seen between the RMC models based on the neutron diffraction data and those based on the X-ray diffraction data. These are most pronounced in g_{SiLi} and g_{LiLi} , since there the higher sensitivity of the neutron probe to the lithium ions becomes particularly relevant. Generally one should expect that due to the different weighting factors of the neutron and X-ray scattering probes, the combination of both in the simulated data will give the best results. Indeed, we find that the RMC models for which both the neutron and the X-ray diffraction data were used, show the best agreement with the MD data.

As a simple measure for comparison of all RMC models with the MD model, we introduce the integral

$$d_{ij}^z = \int |g_{ij}^z(r) - g_{ij}^{\text{MD}}(r)| dr \quad (7)$$

over the difference between the partial radial distribution functions of the RMC model α and the MD system. In the numerical calculation we integrated up to $r = 10$, which amounts to an integration to infinity, since $g_{ij}^z(r) \cong g_{ij}^{\text{MD}}(r) \cong 1$ for $r \gtrsim 10$. The results shown in Table 5 allow us to quantify the quality of the RMC models α relative to each other by means of the single number d_{ij}^z for each partial radial distribution function $g_{ij}(r)$. Note that this number only gives a general trend, but does not specifically account for deviations in particular structural features, such as, for example, offsets in certain peak and minima positions. It is surprising that on average the IC and IR models that are not refined against

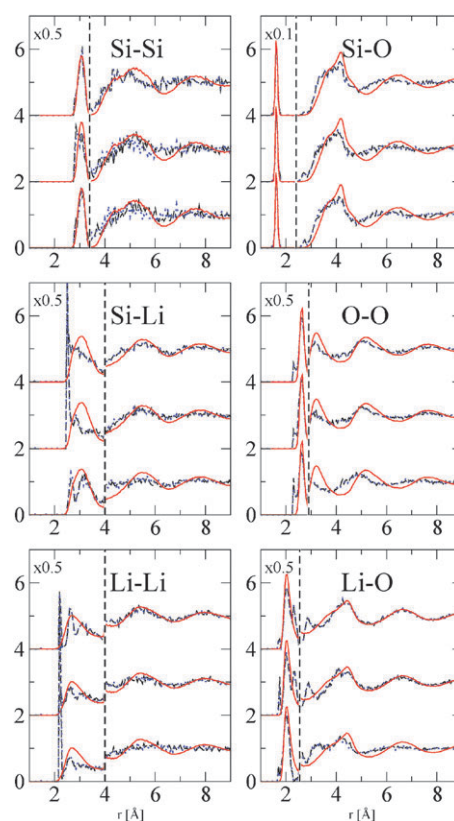


Fig. 3 Comparison of $g_{ij}(r)$ of $\text{Li}_2\text{O-SiO}_2$ RMC models based on crystalline-type (dashed line) and random (dotted line) starting configurations with that of a $\text{Li}_2\text{O-SiO}_2$ MD system (solid line). The RMC model based on neutron diffraction data is shown with a vertical offset of 2, while the RMC model based on both neutron and X-ray diffraction data is shown with an offset of 4. In order to show the full first peak, the curves are scaled by the given factor on the left side of the vertical dashed line in each plot.

diffraction data, but just are made compliant with short-range order constraints, are not much worse than the RMC models (XC, XR, NC, NR) refined further against only one diffraction set (X-ray or neutron). For example, the XC model shows an average $d_{ij} = 1.46$ compared to an average $d_{ij} = 2.10$ for the IC model, which amounts to an improvement by 30%.

When the initial RMC models are refined against both the X-ray and neutron diffraction data, the deviations become larger and improvements by 45% are achieved in the average d_{ij} values. We note that this improvement is due to the fact that the NXR model provides quite good agreement for all individual partial radial distribution functions. This does not mean that it necessarily gives better agreement for an individual partial distribution function than one of the other 4 models based on one scattering probe only. For the individual partial distribution functions, the NXR model gives best values only for the O-O and Li-O partial distribution function in Table 5. However, when the refinement is guided by one scattering probe only, large deviations occur for certain partial radial distribution functions (see, for example, the d_{SiLi} for the NC and NR models, or the d_{LiLi} values for the XC and XR models).

Table 5 Integrated differences d_{ij}^z of partial radial distribution functions, cf. eqn (7)

Pair	XC	XR	NC	NR	NXR	IC	IR	C
Si-Si	1.10	1.24	1.42	1.50	1.21	1.56	1.56	9.76
Si-O	1.25	1.29	1.44	1.44	1.28	3.58	3.47	6.58
Si-Li	1.47	1.52	2.36	2.27	1.53	1.63	1.83	9.84
O-O	1.44	1.47	1.03	0.99	0.88	2.29	2.21	5.93
Li-Li	2.03	2.01	1.05	0.97	1.14	1.51	1.58	9.75
Li-O	1.46	1.42	1.24	1.12	0.91	2.01	2.04	6.71
Average	1.46	1.49	1.42	1.38	1.16	2.10	2.12	8.10

4.2 Coordination numbers

The first neighbor shell coordination number distributions $f_{ij}(N)$ are defined here as the fractions of atoms of type i which have N atoms of type j within a first neighbor shell radius r_{ij} . These radii can be identified by the position of the first minimum of the partial radial distribution functions $g_{ij}(r)$ shown in Fig. 3. Note that being neighbors in the sense of this analysis is not associated with having a chemical bond. To quantify the quality of the various RMC models α , the overlap

$$\phi_{ij}^{\alpha} = 1 - \sum_{N=0}^{\infty} |f_{ij}^{\alpha}(N) - f_{ij}^{\text{MD}}(N)|. \quad (8)$$

was calculated. A value $\phi_{ij}^{\alpha} = 1$ means perfect overlap between the distributions of the coordination numbers $f_{ij}^{\alpha}(N)$ and $n_{ij}^{\text{MD}}(N)$ of the RMC model α and the MD structure.

The results are summarized in Table 6. No significant differences in the ϕ_{ij}^{α} are found between the RMC models based on the crystalline-type starting configuration and the random starting configuration (with one exception for Si-Li, where a larger difference is observed between the RMC-XC and RMC-XR models). This suggests that the quality of reproducing coordination numbers is independent of the starting configuration. A significant difference between the neutron based and the X-ray based RMC models is found in the Li-O coordination numbers, where the better quality for the neutron based model can be traced back to the higher sensitivity of neutrons to Li. An improved overall agreement is achieved when using both X-ray and neutron diffraction data, though the two most significant discrepancies (Si-Si and O-O) are still there. It is also informative to take a look at the overlap numbers of the initial models that are based on the constraints only. These are comparable in quality with the RMC models, which in addition take into account the information from one scattering probe. As for the partial radial distribution functions discussed in the previous section 4.1, the RMC-NXR shows a clear improvement compared to the initial RMC models IC and IR.

Fig. 4 shows a detailed comparison of the coordination number distributions of the RMC-NC and RMC-XC models with the MD model. For the distribution $f_{\text{SiO}}(N)$ not shown in Fig. 4, we obtained a very good agreement which essentially results from the constraint that silicon atoms must have 4-fold coordination. The most striking discrepancies between the RMC models and the MD structure are found in $f_{\text{OO}}(N)$ and $f_{\text{SiSi}}(N)$. The MD model shows a clear bimodal distribution with maxima at 3 and 6 neighbors (corresponding to non-bridging oxygens and bridging oxygens) in $n_{\text{OO}}^{\text{MD}}(N)$,

Table 6 Overlap of coordination numbers in percent (see eqn (8)); first neighbor shell radii are given in the second column

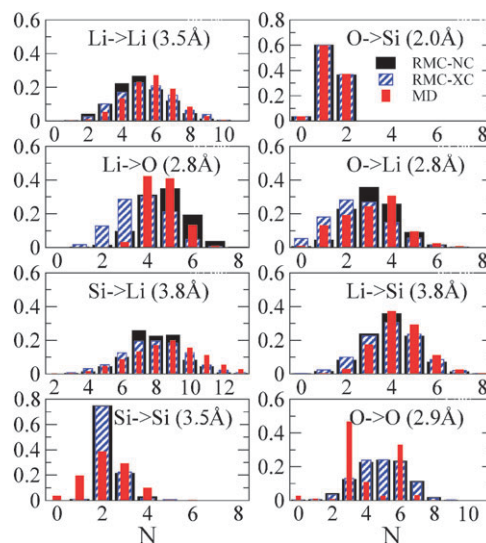
Pair	$r_{ij}/\text{\AA}$	XC	XR	NC	NR	NXR	IC	IR	C
Si-O	2.0	98.4	98.8	99.7	98.4	95.4	99.7	98.8	93.2
O-Si	2.0	99.5	99.6	99.5	99.6	99.1	99.6	99.6	91.2
Li-O	2.8	69.8	68.2	83.0	85.1	87.7	69.3	69.8	48.8
O-Li	2.8	84.5	82.5	84.9	84.9	86.6	83.1	84.5	57.6
Si-Li	3.8	90.4	80.9	77.8	78.5	83.8	80.6	74.5	47.7
Li-Si	3.8	89.5	87.9	87.1	86.7	89.2	84.7	81.7	49.0
Si-Si	3.5	64.0	65.1	64.5	61.9	62.3	66.0	64.1	63.9
O-O	2.9	52.9	52.0	54.2	54.3	58.9	51.6	51.1	89.9
Li-Li	3.5	82.4	81.5	79.5	81.2	92.8	84.4	84.9	52.6
Average	—	81.3	79.6	81.1	81.2	84.0	79.9	78.8	66.0

while the RMC models have a broad smooth distribution. On the other hand, $n_{\text{SiSi}}^{\text{RMC}}(N)$ is much narrower than $n_{\text{SiSi}}^{\text{MD}}(N)$. These findings suggest that the short-range order of the RMC models corresponds quite well to that of the MD structure, but that the medium-range order, and particularly the structure of the Si-O network, has significant differences. We note, that there are virtually no differences between $f_{\text{SiSi}}(N)$ and $f_{\text{OO}}(N)$ among the five RMC models.

In summary, we can conclude that most features in the coordination number distribution are already captured by the constraints. This may not be surprising, since coordination numbers for Si and O have been used as input requirements together with the rather high density of the system. As a consequence, there is not much freedom for the coordination numbers between other types of ion pairs.

4.3 Bond-angle distribution

We calculated bond-angle distributions for intra-tetrahedral angles (O-Si-O) and inter-tetrahedral angles (Si-O-Si) and found that all RMC models have essentially the same bond-angle distributions. Differences lie within the statistical spread.

**Fig. 4** Comparison of histograms of coordination numbers of $\text{Li}_2\text{O-SiO}_2$ for RMC models based on a crystalline-type starting configuration using neutron diffraction data (black solid wide bars) and X-ray diffraction data (striped bars), and the original MD structure (narrow solid bars). The first atom type is the center atom, and the given distances are the radii of the coordination sphere.

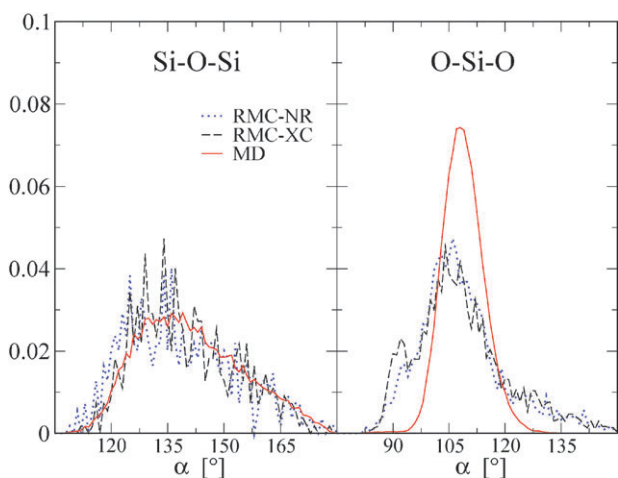


Fig. 5 Bond-angle distributions of the MD structure (solid lines) and RMC models based on a crystalline-type starting configuration using neutron diffraction data (dotted lines) as well as based on a random starting configuration using X-ray diffraction data (dashed lines). In the left panel the distributions of intra-tetrahedral angles (O-Si-O), and in the right panel the distributions of inter-tetrahedral angles (Si-O-Si) are shown.

In Fig. 5 the distributions for the RMC-NR and RMC-XC model are compared to that of the MD structure. The Si-O-Si bond-angle distribution of the RMC models agrees well with the MD data. The intra-tetrahedral bond-angles, on the other hand, are much broader distributed in the RMC models than in the MD structure. This impression can be quantified by calculating the mean angles $\bar{\alpha}(\text{Si-O-Si})$ and $\bar{\alpha}(\text{O-Si-O})$ as well as the standard deviations $\Delta\alpha(\text{Si-O-Si})$ and $\Delta\alpha(\text{O-Si-O})$. It is found that the mean angles of all RMC models agree very well with the MD values, while the standard deviations are larger by a factor of two, see Table 7. This finding corresponds to the deviations observed in the partial radial distribution functions in Fig. 3 and the coordination number distribution of O-O in Fig. 4. There, distinctive features of the MD data, as the second peak in $g_{\text{OO}}^{\text{MD}}$ and the bimodal distribution in $f_{\text{OO}}^{\text{MD}}$, are not well reproduced by the RMC models.

4.4 Ring-size distribution

In order to compare the topology of the glass-network we determined ring-size distributions for each model. Here rings and their size are defined in the following manner:

- (i) A Si-atom and an O-atom are considered neighbors if their distance is smaller than 2.0 Å (using minimum image convention).
- (ii) For each Si-atom γ , the smallest closed loop of alternating neighboring silicon and oxygen atoms is determined, which entails the Si-atom γ .

(iii) A smallest loop is counted as a ring if the sum of bond vectors in the loop is zero.³¹

(iv) The size of the ring is equal to the number of its Si-atoms.

The maximum number of rings equals the total number of Si-atoms. However the number of rings is generally smaller, since there are a number of Si-atoms for which no ring is found (e.g., for an isolated SiO_4 tetrahedra), and two different Si-atoms can be associated with the same ring.

In Fig. 6 we plot the number of rings per volume as a function of the ring size for the MD system, the RMC-NC and the RMC-NR-model. No data is shown for the X-ray and combined data based RMC models, since their ring-size distributions are practically the same as for the neutron diffraction data based RMC models. Indeed the ring-size distributions almost do not change compared to those of the initial models. On the other hand, there is a clear dependence upon the starting configurations. While most rings (40%) of the RMC-NR model are of size three and four, the RMC-NC model has a high number of rings of size 4 and 6. The latter is more in line with what is found in the MD system.

When removing rings due to requirement (iii) we noticed that the RMC-NC and the RMC-XC models have a very high number of rejected smallest loops, where the components of the bond vector sum are integer multiples of the box length L . Examining these loops in more detail reveals that they are often straight linear chains penetrating the system parallel to a coordinate axis (see also Fig. 7). Such straight chains are not found in the RMC-NR and the RMC-XR models and in the MD structure. In these models there occur also rejected loops, but their number is much smaller and they are more twisted than in the RMC models based on the crystalline starting configurations.

5. Summary and conclusions

The RMC method successfully reproduces many salient features of the local structure of the original MD system. Some differences are found in the partial radial distribution function of O-O, and in the coordination number distributions of Si-Si and O-O. With respect to the structure beyond nearest neighbor distances the RMC models are less sensitive and therefore cannot be expected to capture the medium range order in all details.

Comparing RMC models based on X-ray and neutron scattering data revealed no significant differences. Moreover, we found that the additional consideration of scattering data from one type of probe (either X-ray or neutron) gives only a modest improvement over the initial RMC models that are based on geometric constraints only (number density, minimal pair distances, some coordination numbers). When including

Table 7 Mean values and standard deviations of bond angles

	MD	XC	XR	NC	NR	NXR	IC	IR	C
$\bar{\alpha}(\text{Si-O-Si})$	141.2	139.8	140.7	137.4	138.6	140.5	138.0	138.5	125.7
$\Delta\alpha(\text{Si-O-Si})$	13.7	13.1	13.6	14.5	14.5	13.1	14.9	15.5	0.5
$\bar{\alpha}(\text{O-Si-O})$	108.8	108.7	108.7	108.7	108.8	109.0	108.2	108.2	108.9
$\Delta\alpha(\text{O-Si-O})$	5.9	13.1	12.9	12.7	12.4	11.3	15.6	15.9	3.2

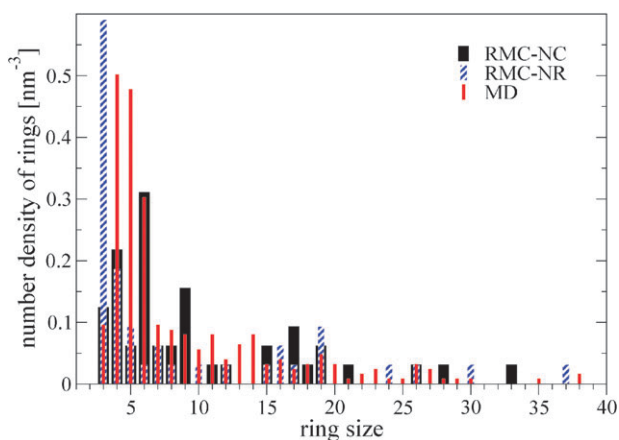


Fig. 6 Comparison of ring size distributions of $\text{Li}_2\text{O-SiO}_2$ RMC models based on a crystalline type starting configuration using neutron diffraction data (black wide bars) and based on a random starting configuration (striped bars) with that of a $\text{Li}_2\text{O-SiO}_2$ MD system (narrow bars).

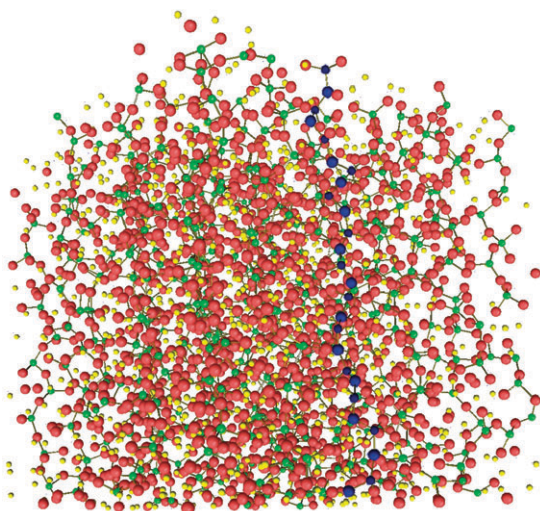


Fig. 7 Picture of the RMC model based on a crystalline-type starting configuration. Lithium atoms are marked as small yellow spheres, silicon atoms as medium sized green spheres, and oxygen atoms as large red spheres. In the center a linear chain of neighboring Si and O is marked in dark blue, which is a leftover of the starting configuration.

both scattering probes, however, the input information for the RMC modeling becomes larger due to the different weighting factors in eqn (4) for the two scattering probes. As a consequence a significant improvement of the initial RMC models is achieved.

Most structural properties of the RMC models do not depend much on the type of starting configuration (crystalline or random). Even the ring-size distributions do not differ that much. However, taking a closer look at the rings, revealed that the RMC models based on the crystalline starting configuration exhibit straight linear chains penetrating the system. These straight chains are remnants of the crystalline starting configuration and their occurrence is not reflected in the other structural properties studied. In particular, there are

no differences in $G(r)$ and $S(Q)$ between the RMC models based on the crystalline and the random starting configuration. These findings show that one should check carefully if a medium-range order feature of interest in RMC models is only a product of a particular starting configuration or if it can be reproduced using totally different starting configurations. Generally the RMC should become independent of the starting configuration when using larger weighting factors for transient time intervals (corresponding to a type of “simulated annealing”) or when using very long simulation times. However, in order to check what is “long enough” requires care. Further methodological work is necessary to endow RMC simulations with capabilities of capturing better the medium-range order features in heavily disordered materials since those features, as a rule, are not very well expressed in the diffraction data which typically guide the simulations themselves.

Work on this project was supported in the Materials World Network by the Deutsche Forschungsgemeinschaft (DFG Grant number MA 1636/3-1) and by the NSF (NSF DMR Grant number 0710564).

Appendix: RMC algorithm

Three types of experimental data were considered to contribute to the effective Hamiltonian $H_{\text{eff}} = \sum_{\alpha} \chi_{\alpha}^2$, $\chi_{\alpha}^2 = \tilde{\chi}_{\alpha}^2 / \sigma_{\alpha}^2$, in eqn (6):

The χ_S^2 for the structure factor $S(Q)$ reads

$$\chi_S^2 = \sum_i \frac{[S^c(Q_i) - S^e(Q_i)]^2}{\sigma_S^2}, \quad (9)$$

where S^e is the experimental structure factor, S^c is the structure factor calculated in the RMC configurations, Q_i are the wave vectors for which S^e was measured, and σ_S is the chosen tolerance (σ_S was chosen independent of Q with the value given in Table 4).

The χ_g^2 for the radial distribution function $G^c(r)$ reads:

$$\chi_g^2 = \sum_i \frac{[G^c(r_i) - G^e(r_i)]^2}{\sigma_g^2}, \quad (10)$$

where G^e and G^c are, respectively, the experimental and the calculated radial distribution functions, r_i are the distances for which G^e was determined from S^e , and σ_g is the tolerance (σ_g was chosen to independent of r with the value given in Table 4).

The $\chi_{\alpha,\beta;k}^2$ for the coordination number constraints, *i.e.* for the fractions of four-fold coordinated Si ($\alpha = \text{Si}$, $\beta = \text{O}$, $k = 4$), bridging O ($\alpha = \text{O}$, $\beta = \text{Si}$, $k = 2$), and non-bridging O ($\alpha = \text{O}$, $\beta = \text{Si}$, $k = 1$), read

$$\chi_{\alpha,\beta;k}^2 = \frac{[f_{\alpha,\beta}^c(k) - f_{\alpha,\beta}(k)]^2}{\sigma_{\alpha,\beta;k}^2}. \quad (11)$$

Here $f_{\alpha,\beta}(k)$ are the required fractions ($f_{\text{SiO}}(4) = 1$, $f_{\text{OSi}}(2) = 0.37$, $f_{\text{OSi}}(1) = 0.63$) and $f_{\alpha,\beta}^c(k)$ are the calculated fractions in the RMC configurations. The chosen weighting factors $\sigma_{\alpha,\beta;k}$ are given in Table 4.

References

- 1 R. L. McGreevy and L. Pusztai, *Mol. Simul.*, 1988, **1**, 359.
- 2 H. Uhlig, M. J. Hoffmann, H. P. Lamparter, F. Aldinger, R. Bellissent and S. Steeb, *J. Am. Ceram. Soc.*, 1996, **79**, 2839.
- 3 M. Fabian, P. Jovari, E. Svab, G. Meszaros, T. Proffen and E. Veress, *J. Phys.: Condens. Matter*, 2007, **19**, 335209.
- 4 W. Yao, S. W. Martin and V. Petkov, *J. Non-Cryst. Solids*, 2005, **351**, 1995.
- 5 D. L. Messurier, V. Petkov, S. W. Martin, Y. Kim and Y. Ren, *J. Non-Cryst. Solids*, 2009, **355**, 430.
- 6 R. L. McGreevy, *J. Phys.: Condens. Matter*, 2001, **13**, R877.
- 7 L. Pusztai and G. Toth, *J. Chem. Phys.*, 1991, **94**, 3042.
- 8 L. Pusztai, H. Dominguez and O. A. Pizio, *J. Colloid Interface Sci.*, 2004, **277**, 327.
- 9 A. de Santis and D. Rocca, *Mol. Simul.*, 1996, **17**, 143.
- 10 S. Kohara and K. Suzuya, *J. Phys.: Condens. Matter*, 2005, **17**, S77.
- 11 Y. Murakami, T. Usuki, S. Kohara, Y. Amo and Y. Kameda, *J. Non-Cryst. Solids*, 2007, **353**, 2035.
- 12 V. Petkov and D. Le Messurier, *J. Phys.: Condens. Matter*, 2010, **22**, 115402.
- 13 M. Fabian, E. Svab, T. Proffen and E. Veress, *J. Non-Cryst. Solids*, 2008, **354**, 3299.
- 14 S. Adams and J. Swenson, *Phys. Rev. Lett.*, 2000, **84**, 4144.
- 15 J. Swenson and S. Adams, *Phys. Rev. Lett.*, 2003, **90**, 155507.
- 16 C. Müller, E. Zienicke, S. Adams, J. Habasaki and P. Maass, *Phys. Rev. B: Condens. Matter Mater. Phys.*, 2007, **75**, 014203.
- 17 The RMC modeling is done with weighting factors (see below) that are commonly used in connection with measurements. We deliberately divided the work between our two groups: the RMC modeling based on the total structure factors obtained from the MD simulations was performed at Central Michigan University with a typical procedure used for the analysis of experiments and without knowledge of the atomic configurations generated by the MD, which was conducted at TU Ilmenau/University of Osnabrück. In this way we evaluated the RMC modeling as it is commonly used in practice.
- 18 J. Habasaki and I. Okada, *Mol. Simul.*, 1992, **9**, 319.
- 19 J. Habasaki, I. Okada and Y. Hiwatari, *J. Non-Cryst. Solids*, 1995, **183**, 12.
- 20 R. Banhatti and A. Heuer, *Phys. Chem. Chem. Phys.*, 2001, **3**, 5104.
- 21 A. Heuer, M. Kunow, M. Vogel and R. Banhatti, *Phys. Chem. Chem. Phys.*, 2002, **4**, 3185.
- 22 S. J. Plimpton, *J. Comput. Phys.*, 1995, **117**, 1, <http://lammmps.sandia.gov/>.
- 23 D. A. Keen, *J. Appl. Crystallogr.*, 2001, **34**, 172.
- 24 V. F. Sears, *Neutron News*, 1992, **3**, 26, <http://www.ncnr.nist.gov/resources/n-lengths/>.
- 25 C. T. Chantler, K. Olsen, R. A. Dragoset, J. Chang, A. R. Kishore, S. A. Kotochigova and D. Zucker, 2005, <http://physics.nist.gov/ffast> [2009, June 2], originally published in ref. 25 and 26.
- 26 C. Chantler, *J. Phys. Chem. Ref. Data*, 1995, **24**, 71.
- 27 C. Chantler, *J. Phys. Chem. Ref. Data*, 2000, **29**, 597.
- 28 G. Evrard and L. Pusztai, *J. Phys.: Condens. Matter*, 2005, **17**, S1.
- 29 This starting configuration does not correspond to a fully random arrangements of the ions, but to a quasi-random sequential setup, where one after each other the silicon ions, the oxygen ions and the lithium ions are placed into the simulation box under consideration of the minimum distance and coordination number constraints. Details of this setup procedure are described in section 9.8.2. of the manual of the RMCA program, see ref. 29.
- 30 RMC++ manual, <http://www.szfk.hu/~nphys/rmc++/docs.html> (June 2009).
- 31 Without this requirement, chain-like structures penetrating the system can be misinterpreted as rings due to the periodic boundary conditions.